Global mapping reveals more intensively exploited inland than coastal wetlands

Lian Feng (lianfeng619@gmail.com)
Southern University of Science and Technology https://orcid.org/0000-0002-4590-3022
Yang Xu
Southern University of Science and Technology
Hongwei Fang
Southern University of Science and Technology
Xiao-Peng Song
University of Maryland, College Park, MD, US https://orcid.org/0000-0002-5514-0321
Fabian Gieseke
University of Münster, University of Copenhagen
Ankit Kariryaa
University of Copenhagen https://orcid.org/0000-0001-9284-7847
Stefan Oehmcke
University of Copenhagen
Luke Gibson
Southern University of Science and Technology https://orcid.org/0000-0002-7706-3355
Xiating Jiang
Southern University of Science and Technology
Ruimin Lin
Southern University of Science and Technology
Wang Xu
Shenzhen Ecological and Environmental Monitoring Center of Guangdong Province
Chunmiao Zheng
Southern University of Science and Technology https://orcid.org/0000-0001-5839-1305
Martin Brandt
Københavns Universitet https://orcid.org/0000-0001-9531-1239
Rasmus Fensholt
University of Copenhagen https://orcid.org/0000-0003-3067-4527

Article

Keywords:

Posted Date: December 13th, 2022

DOI: https://doi.org/10.21203/rs.3.rs-2353047/v1

Abstract

Losses of coastal wetlands have been observed worldwide, but the extent to which inland wetlands have been exploited by humans is currently unknown on a global scale. Here, we map the distribution of land reclamation over global inland and coastal wetlands using high-resolution satellite observations. Results show that the total area of reclaimed wetlands was 132,886 km^2 globally, with about 2/3 contributed from inland wetlands. From 1984 to 2020, the net gain of reclaimed inland wetlands (26,385 km^2) was 1.6 times that of coastal wetlands (16,371 km^2), due primarily to reduced coastal exploitation in the last decade. We identified significant contributions of wetland reclamation to fishery production, and further revealed greater reclamation rates within than outside protected areas. Our study highlights that the more intensively reclaimed inland wetlands should be highly prioritized, and our global synthesis provides a critical benchmark for assessing potential consequences of wetland exploitation and for future restoration efforts.

Main Text

Inland and coastal wetlands have been exploited for centuries, to accommodate anthropogenic pressures for food security and urban development[1,2]. These exploited wetlands were mainly reclaimed for agricultural or aquacultural purposes (Extended Data Fig. 1); although with apparent socio-economic benefits, they could also cause potential environmental and ecological consequences, such as biodiversity loss and water quality deterioration[3,4]. For example, reclamation has caused a 73% reduction of mangrove coverage in China in the past fifty years[5], causing a substantial loss of carbon stocks, increasing the risks of coastal erosion, and threatening the habitats of various aquatic organisms[6–9]. Almost all of the world's freshwater consumption and > 40% of all living species rely on wetlands, yet the rate of wetland loss is reported to be three times faster than forests[10]. This calls for an urgent need for a better understanding of the conflict between socio-economic development and the eco-environmental safety of wetland ecosystems.

Detailed characterization of land-use transformations over global wetlands is the first step toward future strategies for the sustainable management of natural resources. Recently, high-resolution satellite-based maps of the extent and dynamics of marine coastal wetlands, such as tidal flats, mangroves, and salt marshes, have become available[11–13]. Previous studies have utilized these datasets to achieve a consensus on the overall degradation of global coastal wetlands[4,14,15]. However, it is challenging to further differentiate undisturbed natural wetlands from those converted into agricultural lands or aquaculture ponds, which all could be seasonally inundated and with vegetation growth, hitherto hindering accurate assessments of their distinct ecosystem functions. Furthermore, the reclamation of lakes and river floodplains was also reported worldwide[1,16], and could potentially cause more immediate adverse impacts on humans (such as floods) than the reclamation of coastal wetlands[17]. However, the extent to which inland wetlands have been developed is currently unknown on a global scale.

Here, we applied a deep learning method to identify human-reclaimed areas over global inland and coastal wetlands using 30-m resolution satellite observations, addressing two fundamental questions: (i) where and how have global inland and coastal wetlands been exploited over the past four decades? and (ii) have exploitation activities intensified within this timeframe? We examine these questions at national, regional, and global scales.

Mapping Reclaimed Areas In Global Inland And Coastal Wetlands

To map human-reclaimed wetlands, we used the Global Surface Water Occurrence (GSWO) dataset[18] and a deep-learning algorithm (see Methods). The GSWO dataset was generated using 4.5 million 30-m resolution Landsat images acquired between 1984 and 2020. For every 30×30-m pixel, the dataset provides a time series of the probabilities of water present within the pixel. An automated deep learning classification algorithm was applied to identify wetlands characterized by evident human modifications (e.g., regular shape boundaries and uniformly arranged patterns) from the GSWO data, reclaimed mainly for agricultural or aquacultural purposes (Extended Data Fig. 1 & Extended Data Fig. 2). Validation using high-resolution images from Google Earth show overall accuracies of > 90% for the classification of reclaimed wetlands (Extended Data Table 1), with similar performance for both inland and coastal wetlands. Here, we define coastal wetlands as regions within 30 km of distance from the coastline and with a surface water connection to the sea. We applied the algorithm to water occurrence data during three time periods (1984–2000, 2001–2010, and 2011–2020), and used their combined area as the total area of reclaimed wetlands over the past four decades. We further gridded the data into 1°×1° grid cells, and analyzed the associated long-term changes across three time periods.

Spatial Patterns

A total of 132,886 km^2 of wetlands have been reclaimed globally, of which 85,762 km^2 (64.5%) and 47,124 km^2 (35.5%) were located in inland and coastal regions, respectively (Fig. 1). Most wetlands reclamations are found in low elevation (< 10 m, Extended Data Fig. 3) and are distributed within the latitudinal band of 5°S-40°N. Freshwater lakes were hotspots of human exploitation, representing 58.4% of the total area of transitioned inland wetlands.

Global wetland reclamation was primarily found in Asia, accounting for 65,095 km^2 (75.9%) and 40,618 km^2 (86.2%) of total inland and coastal areas, respectively. Almost all countries in South and Southeast Asia experienced intensive human exploitation along coastlines, with marked reclamations also identified in low-altitude inland regions (Extended Data Fig. 3). As a result, 8 of the 10 countries with the largest transitioned wetlands were found in Asia (China, Vietnam, Indonesia, India, Thailand, Uzbekistan, Pakistan, and Myanmar), with China alone accounting for 38.1% (40,322 km^2) of the total global transformation (Fig. 2a). These results are consistent with the findings of previous localized studies[1,5]. Unexpectedly, although small in size and with a limited coastline, Vietnam (21,446 km^2) ranked second

globally in transitioned area, with human-transformed wetlands accounting for 6.6% of the country's territory (Fig. 2b). Similar disproportionally large shares of wetland transitions were also found in many other Southeast Asian countries (such as Singapore, Thailand, Cambodia, Myanmar, Indonesia) (Supplementary Table 3).

Intensively reclaimed inland wetlands were also identified in the USA (especially in California, Florida, and alongside the Mississippi River), making it the third largest country of reclaimed wetlands, even though coastal wetlands there were less developed (Fig. 2a). Other heavily exploited regions were found in Mexico (especially along the coast of the Gulf of California), Ecuador (Río Guayas River Delta), Egypt (the Nile River Delta), and Iraq (the floodplain of Tigris-Euphrates river system), highlighting the heterogeneous distributions of human-transformed wetlands and the importance of the synoptic view provided by satellite remote sensing.

Based on the interpretation of global probability samples (see Methods), we estimated the proportions of the two major land-use transformations: paddy fields and aquaculture ponds. Most of the reclaimed wetlands (~ 94%) were used for paddy fields or aquaculture ponds, but their contributions varied by region: paddy fields dominated inland wetlands, while aquaculture dominated coastal wetlands, in both cases representing > 60% of wetland transformations in these respective regions (Extended Data Fig. 4). Areas of wetland reclamation for other purposes (e.g., salt ponds, mine ponds, tailing ponds, treatment plants) were much smaller (~ 6%), but they represent major contributions in Africa (33.1% for inland and 47.2% for coastal regions, respectively). It should be noted that the reclamation types related to dry season paddy rice production and rainy season aquaculture production are practiced in a seasonal rotation scheme in some regions (Extended Data Fig. 1 & Extended Data Fig. 5), posing challenges to differentiate them further.

Long-term Trends

Wetland reclamation showed steady increases in both inland and coastal wetlands across the three time periods of 1984–2000, 2001–2010, and 2011–2020 (Fig. 3). Yet, the net areal gain over inland wetlands (+ 26,385 km^2) was 1.61 times that in coastal areas (+ 16,371 km^2) over the past four decades, and with spatially and temporally divergent patterns.

From 1984–2000 to 2001–2010, the global net gain of reclaimed areas was comparable between inland (+ 12,757 km^2 or + 34%) and coastal (+ 11,842 km^2 or + 53%) wetlands (Fig. 3). The increases in inland water transitions were the result of high expansion rates in Asia (+ 43%), South America (+ 95%), and North America (+ 18%), whereas minor increases were found in Africa and Oceania (both < 2%), and a net loss (-24%) was observed in Europe (Fig. 4a). Meanwhile, the most intensified coastal exploitations were detected in North America (+ 58%) and Asia (+ 59%), while losses of reclaimed wetlands were found along European coastlines (-12%) (Fig. 4b).

From 2001–2010 to 2011–2020, widespread reclamation of inland natural wetlands was found across all six continents, resulting in an areal gain of + 13,628 km^2 (+ 27%) (Fig. 4a). By contrast, the global increases in transitioned coastal wetlands (+ 4,528 km^2 or + 13%) were much smaller than those of the earlier period, due primarily to the substantially decelerated expansion rates in North America and Asia (rates decreased by > 40%), although reclamation expanded in Africa (+ 26%) and Europe (+ 23%) (Fig. 4b).

For all global 1°×1° grid cells, we classified the change trajectory of wetland reclamation within three time periods into five patterns (see Methods): continuous increase, continuous decrease, decrease then increase, increase then decrease, and stable (Fig. 3). Continuous increases were found in 21% and 30% of the global inland and coastal grids, respectively, and the spatial patterns align closely with those of the most intensively exploited regions (such as Asia, USA, and South America) (Fig. 1 & Extended Data Fig. 6). By contrast, recent decreases were identified in some reclamation hotspots (i.e., increase then decrease), which could be due to an increase in the restoration of natural wetlands (Extended Data Fig. 7a-f) or further transition into non-wetlands (Extended Data Fig. 7g-l). The least common pattern detected in grid cells was continuous decrease (< 5%), and was primarily found in Eastern Europe.

Impacts And Implications Of Human-reclaimed Wetlands

Exploitation of wetlands has contributed substantially to the increase of agri-food production over the past decades. Our analysis revealed significant correlations not only between fishery production and total areas of reclaimed aquaculture ponds at the national level (Extended Data Fig. 8a; R = 0.9, $P < 0.05$), but also between the changes in these two variables from 1984–2000 to 2011–2020 (Extended Data Fig. 8b; R = 0.8, $P < 0.05$). Furthermore, the reported larger increase in freshwater aquaculture than mariculture in the past 20 years[19] also agreed with the more intensive exploitation over inland than coastal zones (Fig. 1). In fact, the intensification of wetland reclamation and the associated development of aquaculture played a crucial role in alleviating poverty in various South and Southeast Asian countries[20] and sub-Saharan Africa[21]. Moreover, the substantial wetland conversion into agricultural land (i.e., rice paddies), especially from inland freshwater lakes, supported the increasing food demands of many developing countries[22].

The recently decelerated development of coastal wetlands could be ascribed to the widespread efforts on coastal conservation and restoration[23]. A recent study also detected a rebound of coastal wetlands in China following a national conservation strategy enacted in 2012[24]. We further compared the areal changes in wetland reclamation within and outside global protected areas (defined by the World Database on Protected Areas). The increasing rates of reclaimed areas were found to be even greater within than outside protected areas, for both inland and coastal wetlands and across different periods (Extended Data Fig. 9), which indeed raises some conservation concerns. Although such unexpected patterns did not apply to all countries, our results indicate that the implementation of conservation plans should be improved in the future.

Although providing many socio-economic benefits, transitions of natural wetlands could cause degradation of inland and coastal ecosystem services. In China, freshwater aquaculture in some eastern provinces represents > 20% of the total nutrient pollution, posing threats to drinking water resources. Nutrients released from reclaimed marine ponds to the coastal environment could reach similar levels to those exported from rivers in some highly polluted regions[25,26]. In many other countries and regions, over-intensification of coastal aquaculture has created excessive nutrient enrichments[23], contributing to the emergence of harmful algal blooms that have triggered hypoxia and mass fish mortality events, beach closure and other environmental disasters[27–29]. Moreover, the intensification of coastal aquaculture, mostly in South and Southeast Asia, could increase the potential impacts of sea level rise and extreme weather events on people's livelihoods and the regional economy at large[4,5,30]. Nevertheless, our temporally and spatially detailed maps provide essential baseline information to perform a global-scale assessment of the adverse environmental and ecological consequences of wetland exploitation.

Our study's major contribution and improvement over previous efforts is to provide the first spatially explicit global synthesis of the human footprint on inland and coastal wetlands. Admittedly, the extent to which natural processes (i.e., sea level rise, coastal erosion, storms)[8,9,31] have modulated global wetlands was not discussed here. However, our results reveal the great extent to which humans are modifying wetlands, demonstrating that the exploitation of inland wetlands was more intensive than in coastal zones, especially during the last decade. Compared to the coastal environment, the global environmental impacts of inland wetland loss are understudied and often overlooked by decision-makers[19,23,32], highlighting the urgency of future investigation, management, and mitigation efforts to focus on the especially vulnerable inland wetlands. Furthermore, the International Union for Conservation of Nature (IUCN) has recently set an ambitious target to protect 30% of the planet by 2030[33], and our benchmark is expected to aid in the future designation of new protected areas and in evaluating the effectiveness of this policy.

References

1. Davidson, N. How much wetland has the world lost? Long-term and recent trends in global wetland area. Marine and Freshwater Research **65**, 936–941 (2014).
2. Hansen, M. C. *et al.* Global land use extent and dispersion within natural land cover using Landsat data. Environmental Research Letters **17**, 034050 (2022).
3. Moi, D. A. *et al.* Human pressure drives biodiversity–multifunctionality relationships in large Neotropical wetlands. Nature ecology & evolution **6**, 1279–1289 (2022).
4. Kirwan, M. L. & Megonigal, J. P. Tidal wetland stability in the face of human impacts and sea-level rise. Nature **504**, 53–60 (2013).
5. Jiang, T.-t., Pan, J.-f., Pu, X.-M., Wang, B. & Pan, J.-J. Current status of coastal wetlands in China: degradation, restoration, and future management. Estuarine, Coastal and Shelf Science **164**, 265–275 (2015).

6. Saintilan, N. *et al.* Constraints on the adjustment of tidal marshes to accelerating sea level rise. Science **377**, 523–527 (2022).
7. Thampanya, U., Vermaat, J. E., Sinsakul, S. & Panapitukkul, N. Coastal erosion and mangrove progradation of Southern Thailand. Estuarine, Coastal and Shelf Science **68**, 75–85 (2006).
8. Nienhuis, J. H. *et al.* Global-scale human impact on delta morphology has led to net land area gain. Nature **577**, 514–518 (2020).
9. Tessler, Z. D. *et al.* Profiling risk and sustainability in coastal deltas of the world. Science **349**, 638–643 (2015).
10. Gardner, R. C. & Finlayson, C. in Secretariat of the Ramsar Convention. 2020–2025 (2018).
11. McOwen, C. *et al.* A global map of saltmarshes. Biodiversity Data Journal **5**, e11764 (2017).
12. Giri, C. *et al.* Status and distribution of mangrove forests of the world using earth observation satellite data. Global Ecology and Biogeography **20**, 154–159 (2011).
13. Murray, N. J. *et al.* The global distribution and trajectory of tidal flats. Nature **565**, 222–225 (2019).
14. Murray, N. J. *et al.* High-resolution mapping of losses and gains of Earth's tidal wetlands. Science **376**, 744–749 (2022).
15. Barbier, E. B. A global strategy for protecting vulnerable coastal populations. Science **345**, 1250–1251 (2014).
16. Hou, X. *et al.* Anthropogenic transformation of Yangtze Plain freshwater lakes: patterns, drivers and impacts. Remote Sensing of Environment **248**, 111998 (2020).
17. Tellman, B. *et al.* Satellite imaging reveals increased proportion of population exposed to floods. Nature **596**, 80–86 (2021).
18. Pekel, J.-F., Cottam, A., Gorelick, N. & Belward, A. S. High-resolution mapping of global surface water and its long-term changes. Nature **540**, 418–422 (2016).
19. Naylor, R. L. *et al.* A 20-year retrospective review of global aquaculture. Nature **591**, 551–563 (2021).
20. Belton, B., Bush, S. R. & Little, D. C. Not just for the wealthy: Rethinking farmed fish consumption in the Global South. Global Food Security **16**, 85–92 (2018).
21. Garlock, T. *et al.* A Global Blue Revolution: Aquaculture Growth Across Regions, Species, and Countries. Reviews in Fisheries Science & Aquaculture **28**, 107–116 (2020).
22. Hishamunda, N., Bueno, P., Ridler, N. & Yap, W. *Analysis of aquaculture development in Southeast Asia*. (Food and Agriculture Organization of the United Nations (FAO), 2009).
23. Duarte, C. M. *et al.* Rebuilding marine life. Nature **580**, 39–51 (2020).
24. Wang, X. *et al.* Rebound in China's coastal wetlands following conservation and restoration. Nature Sustainability **4**, 1076–1083 (2021).
25. Wang, J., Beusen, A. H. W., Liu, X. & Bouwman, A. F. Aquaculture Production is a Large, Spatially Concentrated Source of Nutrients in Chinese Freshwater and Coastal Seas. Environmental Science & Technology **54**, 1464–1474 (2020).

26. Zhang, Y., Bleeker, A. & Liu, J. Nutrient discharge from China's aquaculture industry and associated environmental impacts. Environmental Research Letters **10**, 045002 (2015).
27. Michael Beman, J., Arrigo, K. R. & Matson, P. A. Agricultural runoff fuels large phytoplankton blooms in vulnerable areas of the ocean. Nature **434**, 211–214 (2005).
28. Hallegraeff, G. M. *et al.* Perceived global increase in algal blooms is attributable to intensified monitoring and emerging bloom impacts. Communications Earth & Environment **2**, 117 (2021).
29. Breitburg, D. *et al.* Declining oxygen in the global ocean and coastal waters. Science **359**, eaam7240 (2018).
30. Saintilan, N. *et al.* Constraints on the adjustment of tidal marshes to accelerating sea level rise. Science **377**, 523–527 (2022).
31. Kirwan, M. L., Temmerman, S., Skeehan, E. E., Guntenspergen, G. R. & Fagherazzi, S. Overestimation of marsh vulnerability to sea level rise. Nature Climate Change **6**, 253–260 (2016).
32. Gonçalves, D. V. & Hermoso, V. Global goals overlook freshwater conservation. Science **377**, 380–380 (2022).
33. Nicholson, E. *et al.* Scientific foundations for an ecosystem goal, milestones and indicators for the post-2020 global biodiversity framework. Nature Ecology & Evolution **5**, 1338–1349 (2021).

Declarations

Acknowledgments: We thank Google Earth Engine for providing the Global Surface Water dataset.

Funding: This work was supported by the National Natural Science Foundation of China (NOs: 41971304 and 42271322) and by the Support Plan Program of Shenzhen Natural Science Fund under Grant 20200925155151006.

Author contribution: Y. X.: methodology, data processing and analyses, and writing; L. F.: conceptualization, methodology, funding acquisition, supervision, and writing. All authors participated in interpreting the results and refining the manuscript.

Competing interests: Authors declare no competing interests.

Data and materials availabilities: The polygons of human-reclaimed wetlands generated in this study will be provided to the public upon acceptance of this manuscript.

Methods

Global Surface Water (GSW) dataset

The Global Surface Water (GSW) dataset was developed by the European Commission's Joint Research Centre (JRC), and maps the spatio-temporal distribution of surface water at the global scale (60°S – 80°N) using 30-m Landsat imagery acquired from 1984 to 2020[18]. The GSW occurrence (GSWO) provides

the probability of historical water presence (with a range of 0–100%) over the past four decades. We also used the JRC Monthly History Collection (or MHC, version1.3) data to generate the water occurrence for three separate time periods (1984–2000, 2001–2010, and 2011–2020). The MHC data provides monthly classified images over the past four decades, where each 30-m resolution pixel was classified into water, non-water, or no data on a monthly basis. We used the water occurrence images to (i) prepare the training, validation, and testing labels of human-reclaimed wetlands for the classification approach, and (ii) examine changes in global reclaimed wetlands across different periods. The GSW dataset is available at Google Earth Engine (GEE) (website: https://earthengine.google.com/), and the generation of water occurrence for different periods was also performed through GEE.

Classifying human-reclaimed wetlands using deep learning

The human-reclaimed wetlands we mapped here include two major land-use types: paddy fields and aquacultural ponds (Extended Data Fig. 1); other occasional reclamation purposes (e.g., salt ponds, mine ponds, tailing ponds for the industrial mining process, water treatment plants, and stormwater treatment) can also be identified over inland and coastal wetlands. In theory, human-reclaimed wetlands can be determined manually through moderate to high-resolution satellite images[34], due to their distinct features from natural wetlands (i.e., regularly-shaped boundaries and uniformly-arranged patterns) (Extended Data Fig. 1). However, global mapping of reclaimed wetlands has encountered at least two major challenges: 1) spatially and temporally varied inundation conditions, making it difficult to characterize the wetland features using snapshots of satellite images; 2) the spectral features of reclaimed and natural wetlands are similar in many cases (i.e., reclaimed aquacultural ponds vs. natural waters, and crops in paddy fields vs. natural wetland vegetation), posing large uncertainty for image classifications with multispectral satellite observations. Fortunately, the water occurrence dataset, generated using 30 m-resolution historical Landsat images, can resolve these problems and provide insight into the inundation patterns on global surface water[18]. Apart from giving an indicator of differentiating permanent waters, seasonal waters, and land, the water occurrence also magnifies texture differences between human-reclaimed and natural wetlands (Extended Data Fig. 1). As such, we utilized a deep learning-based image segmentation method to determine global reclaimed inland and coastal wetlands using the water occurrence dataset.

Preparing reliable labels is the first step for applying supervised machine learning approaches. In practice, we visually interpreted and manually delineated human-reclaimed wetlands over GSWO images for 133 sites (ranging from 35.8 km^2 to 19795.3 km^2) distributed across different continents. For each site, we drew a box to determine both positive (human-reclaimed wetlands) and negative (others) samples within each box (Extended Data Fig. 2). We additionally selected 131 no-reclamation sites (ranging from 6.0 km^2 to 7886.7 km^2) with only negative samples, because the negative samples in the above 133 sites were insufficient to represent the various types of natural wetlands (e.g., tidal flats, densely-distributed lakes, intertidal zones, and floodplains). When preparing the labels, we also verified their validity using high-resolution Google Earth images. In total, we delineated 15,731.7 km^2 of positive (9,884.94 km^2 for inland

and 5,846.76 km^2 for coastal wetlands) and 85,712 km^2 of negative labels (77,031.69 km^2 for inland and 8,680.31 km^2 for coastal wetlands).

We adopted the U-Net architecture to classify human-reclaimed wetlands, which was initially developed for tree mapping by Brandt et al.[35]. The U-Net is a convolutional neural network (CNN) architecture for fast and precise image segmentations[36]. It incorporates a contracting and an expansive path that is designed explicitly for concatenation with the correspondingly down-sampled feature map from the contracting path (6). The U-Net architecture can combine features from different spatial regions of the image and thus increase the performance of locating areas of interest, and its intelligence in training end-to-end from very few images and allowing the prediction of full context and global locations and texture simultaneously has been demonstrated[36–38].

We adopted the improved settings to the classic U-Net architecture by Brandt et al. (5), including two convolution layers, max pooling, and batch normalization. We further made the following essential adjustments to match our task (Supplementary Table 1):

First, we did not normalize the GSWO images or patches of GSWO images, because the procedure of producing GSWO images already counterweighs the impacts of no data induced by cloud cover and seasonality in data volume[18]. We also omitted the pixel-wise weight maps during training as it was set specially for tree mapping in Brandt et al. (5).

Second, we enlarged the patch size from 256×256 to 512×512 pixels, since larger patches represent more exclusive features of human-reclaimed wetlands. Besides, the patches were sequentially sampled with a 1/4 overlap within boxes instead of using random sampling during training. In some cases, while random sampling made the final model perform well on all sampled patches of the training and validation datasets, the model showed poor generalization performance in independent areas out of these sampled areas. However, sequentially sampling ensured all pixels in boxes could be included in the training procedures, and the 1/4 overlap also allowed that image features at the borders of adjacent patches could be fully learned by the U-Net model.

Third, the piecewise affine, perspective transformation, and linear contrast enhancement in data augmentation were not applied. This is because piecewise affine and perspective transformation tends to distort regularized boundaries of reclaimed wetlands, and linear contrast enhancement could change the water-occurrence range (0%-100%).

Fourth, we developed a new loss function to train the U-Net model. (20). The original form adopted by Brandt et al. (5) was the Tversky loss, which performs well for unbalanced data due to its ability to weigh the penalties of false positives and false negatives during training[39]. However, the Tversky loss only contributes to model training when a batch incorporates at least one patch with positive samples (Eq. (1)). As some of our training images only contain negative samples (such as the additionally prepared 131 boxes), we revised the loss function as follows:

(i) If a batch has positive samples, we used the same Tversky loss as in Brandt et al. (5):

$$Tverskyloss = 1 - \frac{TP}{TP + \alpha * FP + \beta * FN}$$

1

where TP are true positives, FP are false positives, FN are false negatives, respectively, and where α + β = 1 holds for the two weights. The Tversky loss is modulated by changing the weights (α and β) of FP and FN. We finally set α = 0.6 and β = 0.4 in Tversky loss to balance the commission and omission errors.

(ii) If a batch only constitutes negative samples (i.e., TP = 0), the loss function (denoted as *Neg loss*) was designed as follows:

$$Negloss = \frac{\sum_{i=1}^{8} P_i}{N}$$

2

where P_i is the predicted probability for each pixel in all patches of a batch. The closer theP_i to 1, the greater the probability of being predicted as positive. N is the number of pixels. The *Neg loss* aims to reduce the cases that negative samples are incorrectly identified as positive samples in a batch with no positive samples. The combination of the Tversky loss and the Neg loss function balances the focus on positive samples and negative samples, and is applicable when the training dataset has a large number of negative samples.

We split the labels in the 264 boxes into training (50%), validation (30%), and testing datasets (20%) to perform the hyperparameter tuning of the U-Net (Supplementary Table 1), and we monitored the model performance by comparing several performance metrics, including recall, precision, F1 Score, and MIoU (Mean Intersection over Union):

$$Recall = \frac{TP}{TP + FN}$$

3

$$Precision = \frac{TP}{TP + FP}$$

4

$$F1Score = 2 \bullet \frac{Precsion \bullet Recall}{Precision + Recall}$$

5

$$MIoU = \left[\frac{TP}{TP + FP + FN} + \frac{TN}{TN + FP + FN} \right] /2$$

6

where TN are true negatives. After several rounds of hyperparameter tuning, we finalized the trained model with the hyperparameter settings listed in Supplementary Table 1.

Our trained model exhibited a balanced performance in training, validation, and test datasets, as demonstrated by their similar high values in all four accuracy indices (> 0.83, see Supplementary Table 2). Besides these pixel-wised accuracy matrices, we compared the predicted and labeled human-reclaimed areas within 96 randomly selected patches (512×512 pixels) in the testing datasets. The results also demonstrated favorable agreements between these two areal estimates (R^2 = 0.92, root-mean-square error (RMSE) = 5.12 km^2, see Supplementary Fig. 1).

We applied the well-trained U-Net model to global water occurrence maps over three periods (1984–2000, 2001–2010, and 2011–2020) to generate the maps of human-reclaimed wetlands. Then, we adopted an extensive post-processing procedure for potential artifacts on our predicted global maps. For example, the stripes over Landsat 7 ETM + data could also produce straight boundaries similar to human-reclaimed wetlands, and we ensured that all such misclassifications were removed. After post-processing, we converted the global raster maps of human-reclaimed wetlands over three periods into polygons for further analysis.

Reference samples used to assess classification accuracies

We selected 10,553 reference points over high-resolution (sub-meter) Google Earth images to evaluate the accuracy of our mapped human-reclaimed wetlands, where the points were selected through a stratified random sampling strategy[40]. We only sampled one point within a polygon of predicted reclaimed wetlands, and ensured every country with reclaimed wetlands had at least one validation point. Sample points within the polygons of reclaimed wetlands (i.e., positive samples) were randomly selected (i.e., see Supplementary Fig. 2), and negative samples were selected within 1 km buffer zone but outside the polygons. The total positive and negative validation sample points were 5276 and 5277, respectively, and were distributed globally along the coast (5530 points) and within inland areas (5,023 points) (see Supplementary Fig. 2). For each point, we checked all available high-resolution historical images (2011–2020) on Google Earth, and the points would be deemed as reclaimed wetlands if more than half of these images show features of human reclamation. Comparisons between referenced random points and the GSWO-predicted maps showed high accuracy levels in both inland and coastal regions, demonstrated by the high values in users, producers, and overall accuracies (mostly > 90%, see Extended Data Table 1). Note that we only validated the wetland reclamation map in 2011–2020, because high-resolution images were not available in the early period of Google Earth in many regions. Note that, additional uncertainties in our predicted maps could also include the omission errors (> 20%) of seasonal waters for the JRC MHC products[18], leading to underestimates in areas of global reclaimed wetlands (reclaimed paddy fields

often show seasonally-inundated patterns). Thus, our estimate represents an underestimation of the total human reclamation occurring in wetlands.

Analyzing the use of wetland reclamation

When performing the accuracy assessments, high-resolution Google Earth images also helped us to identify the reclamation purposes of the sampled regions (Extended Data Fig. 1). As such, the proportion of the major reclamation purposes could be represented by these global probability samples; this method was also widely adopted by previous land cover studies[14,41]. A total of 2492 and 2242 reference points were predicted as reclaimed inland and coastal wetlands (Extended Data Table 1), respectively, and we further assigned a reclamation type for each point (paddy fields, aquacultural ponds, or others) by visually interpreting the corresponding high-resolution Google Earth images. The points assigned as others include artificial wetlands for various industrial purposes (e.g., salt ponds, tailing ponds for the industrial mining process, mine ponds, and stormwater treatment areas). We calculated the global and continental proportions of three reclamation types in inland and coastal wetlands (Extended Data Fig. 4). We acknowledge that further distinction between paddy fields, aquacultural ponds, and others remains challenging due to the similarities in spectral features and inundation patterns, with the additional difficulty of seasonal rotations between different reclamation purposes found in some regions (Extended Data Fig. 5).

Analyzing global spatial and temporal patterns

To compare the extent and change in human-reclaimed wetlands over inland and coastal regions, the boundaries of coastal and inland wetlands need to be differentiated. We defined coastal wetlands as potentially inundated areas (i.e., water occurrence of $\geq 1\%$) within 30 km of the coast and with a direct water connection to the ocean. Specifically, we used the Open Street Map (OSM) dataset to determine ocean boundaries (the water layers of OSM define global water-related surfaces (60°S − 90°N) at 3sec resolution (~ 90 m at the equator)[42], and we rasterized the associated surface water maps and excluded regions with water occurrence < 1% in the GSWO map or with > 30 km distance from the coast. Then, we determined ocean-connected regions using an 8-neighborhood method[43]. By contrast, all other wetlands outside these pre-defined coastal areas were considered inland wetlands. Note that, the distance used in previous studies to define coastal areas ranged from 1 to 100 km depending on the focus of interest[13,14,44]. Our sensitivity analysis revealed that the reclamation on coastal wetlands was less intensive than inland wetlands even with a distance of 100 km used to define the coastal zone, similar to the results here using 30 km.

We estimated the total area of human-reclaimed wetlands over the past four decades as the combined area of wetland reclamation over all three time periods (1984–2000, 2001–2010, and 2011–2020). We further gridded the global data into 1°×1°cells (see Fig. 1), and examined the areal changes in human-reclaimed wetlands across different time periods. We classified the changing trajectory for each 1°×1°into five patterns: continuous increase, continuous decrease, decrease then increase, increase then decrease,

and stable (see Fig. 3). The area of reclaimed wetlands within a grid cell was considered stable if the areal change between two periods was < 1 km^2. Note that when a human-disturbed wetland was further converted into a non-wetland (i.e., built-up areas or roads) or restored into natural wetlands within one period, it would be excluded from detection in the subsequent period.

We compared the total area of human-reclaimed wetlands and associated changes between inland and coastal regions, and also performed continental and country-level statistics (Fig. 2, Fig. 3, Fig. 4, Supplementary Table 3), using the boundaries provided by the marine region geodatabase (https://www.marineregions.org/downloads.php).

We examined the elevation distribution of human-reclaimed wetlands based on the SRTM elevation data (Extended Data Fig. 3)[42,45]. We further estimated the proportion of reclaimed inland wetlands in lakes, using lake boundaries as defined in the GLAKES dataset[46]; GLAKES provides the maximum extent of > 3 million lakes with a surface area > 0.03 km^2.

Analyzing the potential impacts of wetland reclamation

We examined the potential contribution of wetland reclamation to fishery production by analyzing the correlation between areas of aquacultural ponds and aquacultural production. Country-level aquaculture production data provided by the Food and Agriculture Organization (FAO) of the United Nations was obtained via https://ourworldindata.org/grapher/aquaculture-farmed-fish-production. For each country, we summed the reclaimed areas for inland and coastal wetlands, and then multiplied their corresponding proportions of aquacultural ponds to estimate the total area of aquacultural ponds (Fig. 1). The areas of reclaimed aquacultural ponds were estimated for the overall (1984–2020), the start (1984–2000), and the end (2011–2020) periods. During this calculation, we assumed that the proportions of aquacultural ponds for different countries were the same, and remained stable across different periods. Moreover, the calculations were performed separately for inland and coastal wetlands, due to their different proportions of aquacultural ponds (Fig. 1). Meanwhile, we estimated the mean aquacultural production for different periods (the data for the overall and the end periods were only available through 2018) using datasets from FAO. We analyzed the correlation between maximum aquacultural production and the total area of reclaimed aquacultural ponds at the national level for the overall period (Extended Data Fig. 8a). Then, we further examined the correlation between changes in aquacultural production and changes in reclaimed areas between the start and the end periods (Extended Data Fig. 8b), and such a relationship could be interpreted as the sensitivity of aquacultural production to reclaimed areas of aquacultural ponds. We also attempted to analyze the contribution of reclaimed paddy fields to agricultural production, but such a task is impeded for the following reasons: (1) the identification of cultivated crop type in the reclaimed paddy fields is technically challenging, and therefore, the associated impacts on the agricultural production are difficult to determine. And (2) besides the expansion in arable land, the intensified use of fertilizer and the improvement in irrigation facilities have contributed substantially to the increase in agricultural production in the past decades[47,48].

We further compared the change rates of wetland reclamation within and outside global protected areas between different subperiods (Extended Data Fig. 9), to examine whether the expansion of human reclamation over global wetlands was reduced in established protected areas. The global protected areas were obtained from the World Database on Protected Areas (https://www.protectedplanet.net/en/thematic-areas/wdpa?tab=WDPA), a comprehensive and complete database showing the extent of terrestrial and marine protected areas across the globe.

References

34 Hou, X. *et al.* Anthropogenic transformation of Yangtze Plain freshwater lakes: Patterns, drivers and impacts. *Remote Sensing of Environment* **248**, 111998 (2020).

35 Brandt, M. *et al.* An unexpectedly large count of trees in the West African Sahara and Sahel. *Nature* **587**, 78–82 (2020).

36 Ronneberger, O., Fischer, P. & Brox, T. in *International Conference on Medical image computing and computer-assisted intervention.* 234–241 (Springer, Cham, 2015).

37 Alom, M. Z., Yakopcic, C., Hasan, M., Taha, T. M. & Asari, V. K. Recurrent residual U-Net for medical image segmentation. *Journal of Medical Imaging* **6**, 014006 (2019).

38 Siddique, N., Paheding, S., Elkin, C. P. & Devabhaktuni, V. U-net and its variants for medical image segmentation: A review of theory and applications. *Ieee Access* **9**, 82031–82057 (2021).

39 Salehi, S. S. M., Erdogmus, D. & Gholipour, A. in *International workshop on machine learning in medical imaging.* 379–387 (Springer, Cham, 2017).

40 Singh, A. S. & Masuku, M. B. Sampling techniques & determination of sample size in applied statistics research: An overview. *International Journal of economics, commerce and management* **2**, 1–22 (2014).

41 Song, X.-P. *et al.* Global land change from 1982 to 2016. *Nature* **560**, 639–643 (2018).

42 Yamazaki, D. *et al.* A high-accuracy map of global terrain elevations. *Geophysical Research Letters* **44**, 5844–5853 (2017).

43 Rosenfeld, A. *Digital picture processing*. (Academic press, 1976).

44 Wang, X. *et al.* Rebound in China's coastal wetlands following conservation and restoration. *Nature Sustainability* **4**, 1076–1083 (2021).

45 Farr, T. G. *et al.* The shuttle radar topography mission. *Reviews of geophysics* **45** (2007).

46 Pi, X. *et al.* Mapping global lake dynamics reveals the emerging roles of small lakes. *Nature Communications* **13**, 5777 (2022).

47 Mueller, N. D. *et al.* Closing yield gaps through nutrient and water management. *Nature* **490**, 254–257 (2012).

48 Pingali, P. L. Green revolution: impacts, limits, and the path ahead. *Proceedings of the National Academy of Sciences* **109**, 12302–12308 (2012).

Figures

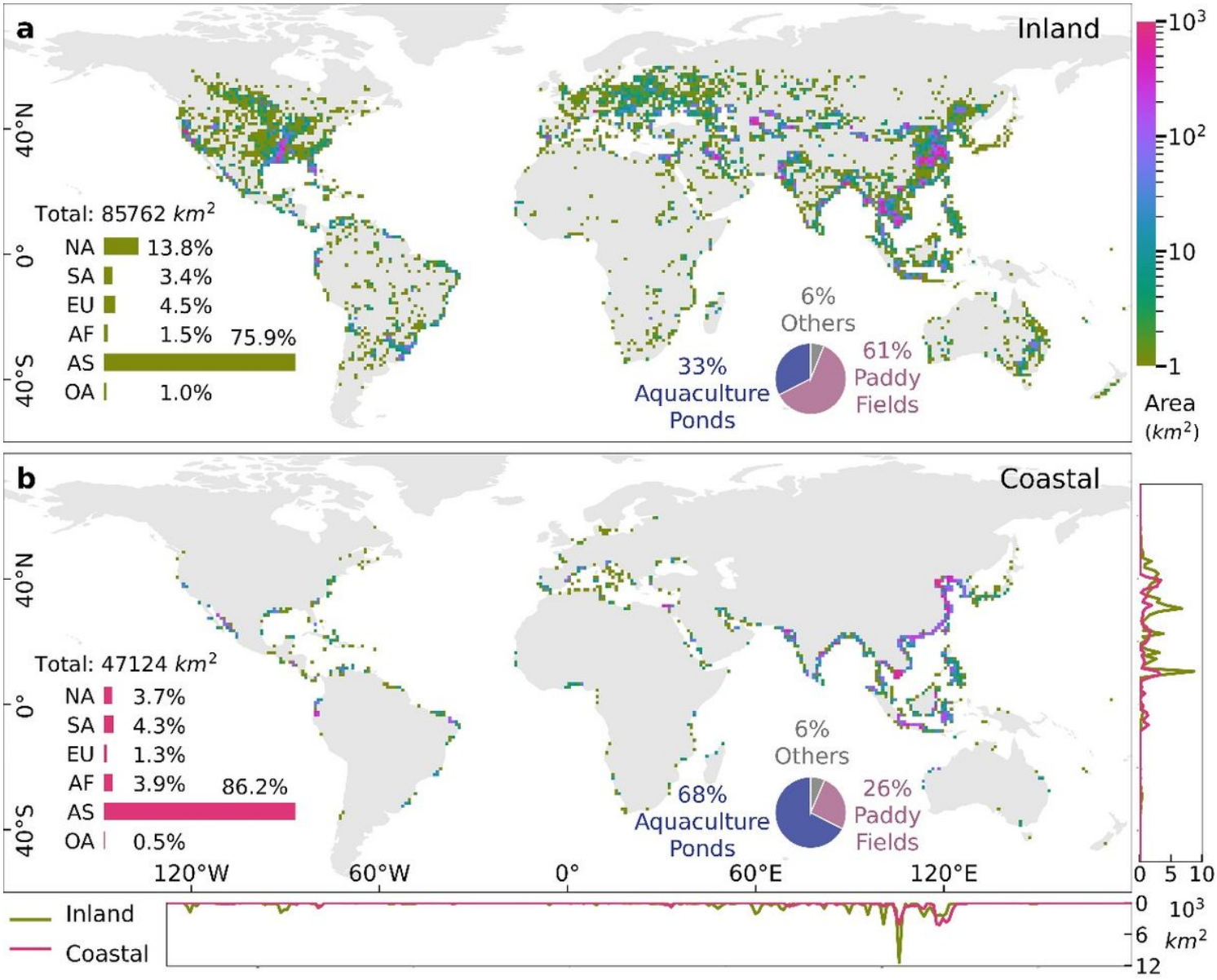

Figure 1

Global patterns of human-reclaimed wetlands from 1984 to 2020. (a) Inland wetlands.**(b)** Coastal wetlands. The data are aggregated into 1°×1° grid cells, and the global total areas and the proportion per continent are presented within each panel. The proportions of different reclamation purposes (aquaculture ponds, paddy fields, and others) are presented using pie charts within the panel. The right

and underside of **(b)** show the 1° latitudinal and longitudinal profiles for both inland and coastal regions. NA: North America, SA: South America, EU: Europe, AF: Africa, AS: Asia, OC: Oceania.

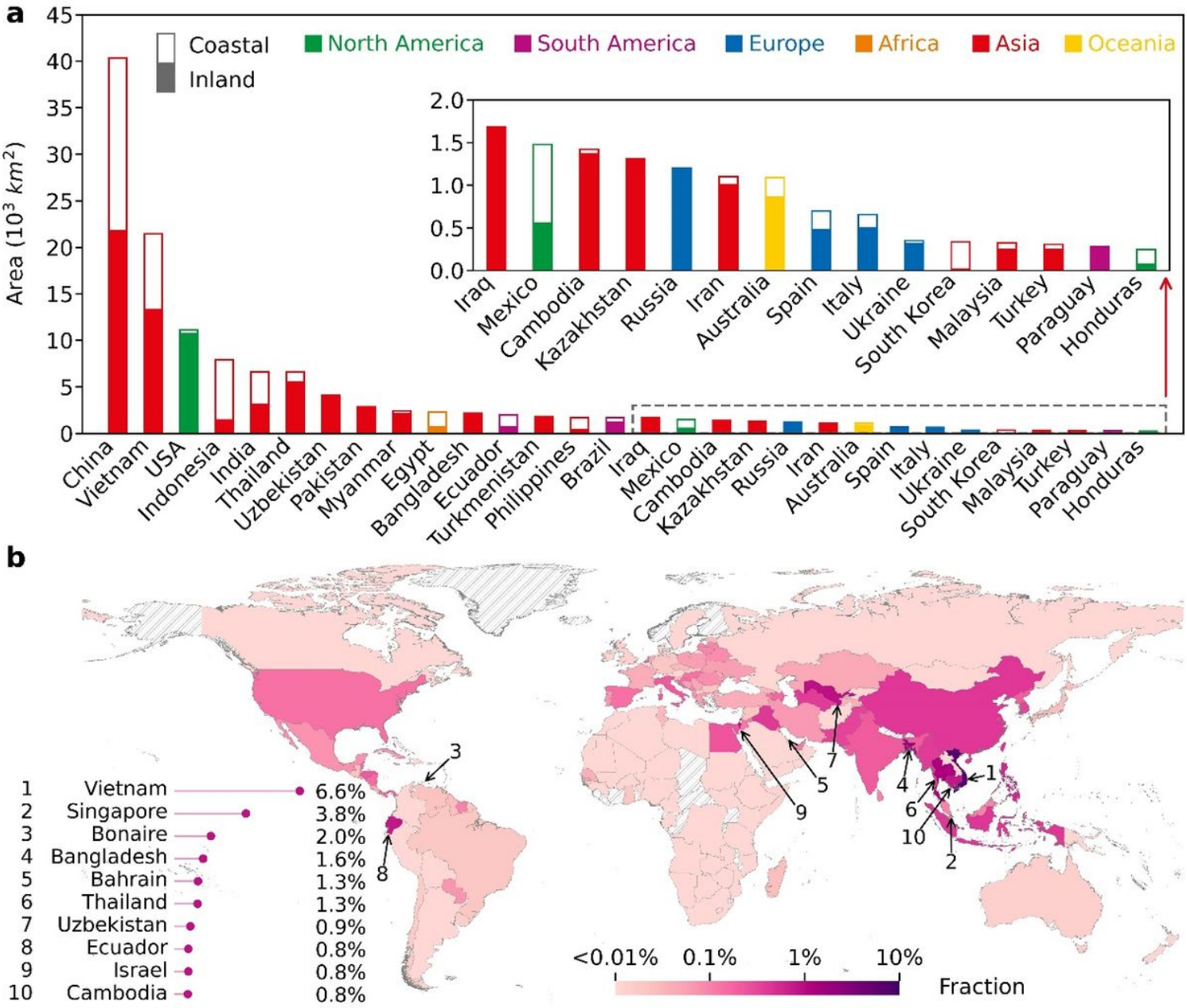

Figure 2

Country-level statistics for human-reclaimed wetlands. (**a**) Top 30 countries for the total area of human-reclaimed wetlands from 1984 to 2020, with the data for lower-ranking countries magnified. Areas of inland wetlands and coastal wetlands are displayed in solid and hollow bars, respectively. (**b**) Fraction of human-reclaimed wetlands to country size. The 10 countries/regions with the highest fractions are presented in the lower left, and their locations are indicated on the global map. Gray-hatched areas indicate countries/regions with no human-reclaimed wetlands detected by satellite.

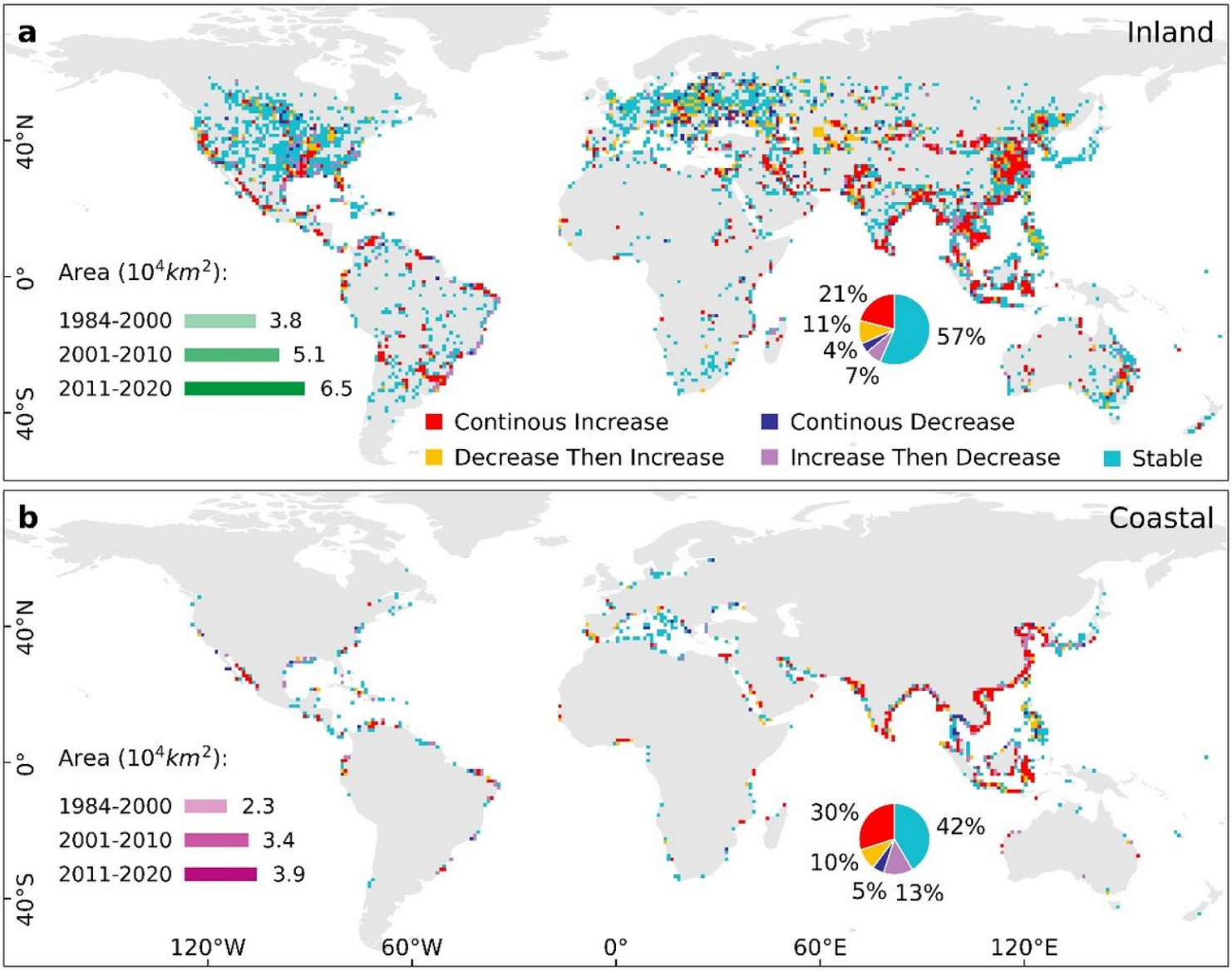

Figure 3

Global patterns of changes in reclaimed wetlands across the three time periods of 1984-2000, 2001-2010, and 2011-2020. (**a**) Inland wetlands. (**b**) Coastal wetlands. The changing trajectory for each 1°×1°grid cell was classified into five types of temporal dynamics: continuous increase, continuous decrease, decrease then increase, increase then decrease, and stable (see Methods). The bar charts present the total human-reclaimed areas for different periods, and the pie charts show the fractions of different changing trajectories.

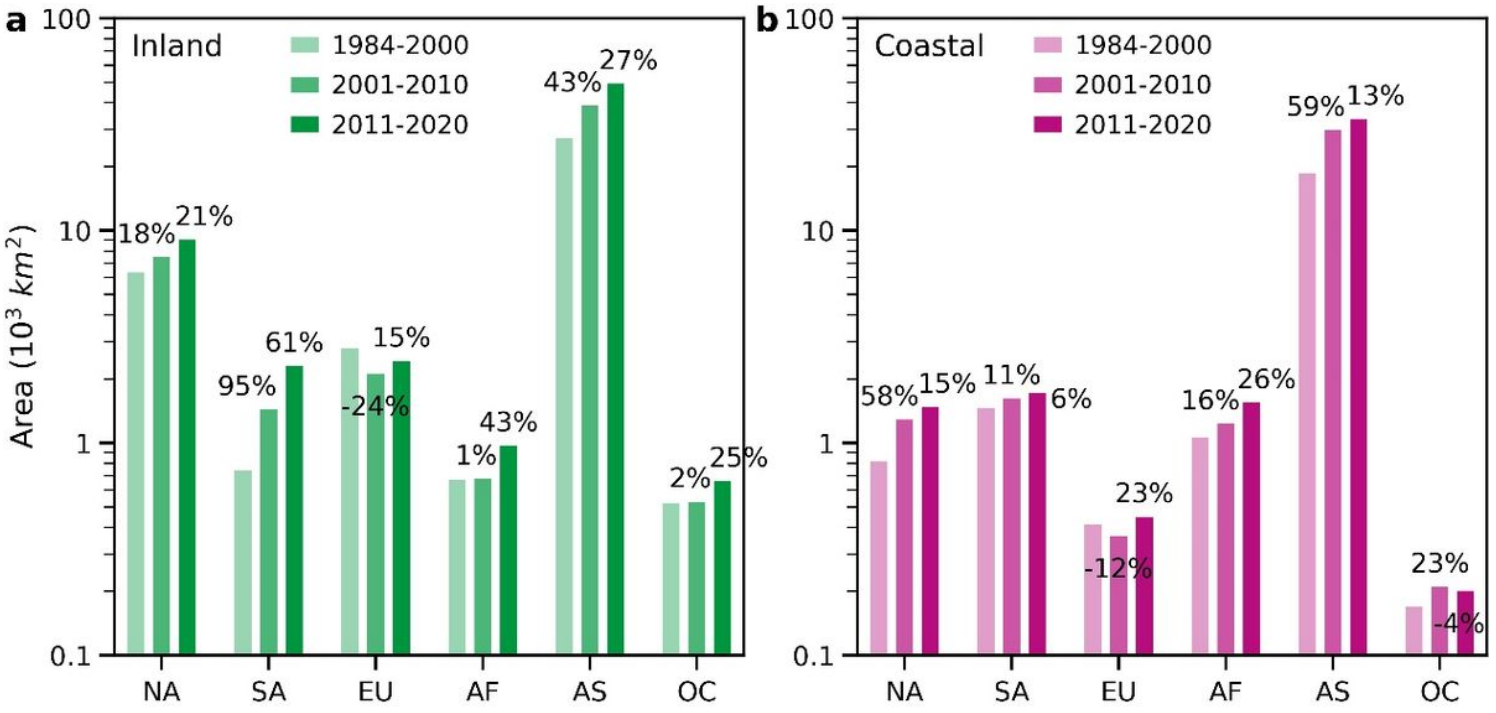

Figure 4

Comparison of the total reclaimed areas within different periods (1984-2000, 2001-2010, and 2011-2020). (**a**) Inland wetlands. (**b**) Coastal wetlands. The annotated numbers (in percentage) are the relative areal changes from the previous to the current period.

Supplementary Files

This is a list of supplementary files associated with this preprint. Click to download.

- Extendeddatafiguresandtables.docx
- SupplementaryTable3.xlsx
- Supplementaryinformation.docx